Chemometrics and Intelligent Laboratory Systems 200 (2020) 103994

Contents lists available at ScienceDirect

Chemometrics and Intelligent Laboratory Systems

journal homepage: www.elsevier.com/locate/chemometrics

Quantitative models for detecting the presence of lead in turmeric using Raman spectroscopy

Putthiporn Khongkaew [a], Chutima Phechkrajang [a], Jordi Cruz [b,*], Vanessa Cárdenas [c], Piyanuch Rojsanga [a]

[a] Department of Pharmaceutical Chemistry, Faculty of Pharmacy, Mahidol University, 447 Sri-Ayuthaya Road, Phayathai, Ratchathewi, Bangkok, Thailand
[b] Escola Universitària Salesiana de Sarrià, Passeig Sant Joan Bosco, 74, 08017, Barcelona, Spain
[c] Universidad del Quindío, Carrera 15 Calle 12 Norte-P.Box, 630004, Armenia, Colombia

ARTICLE INFO

Keywords:
Raman Spectroscopy
Lead
Heavy metals
PLSR
Herbal medicinal products

ABSTRACT

The current study presents a novel methodology to quantify lead in Turmeric using Raman spectroscopy. In this study, Partial Least Squares Regression (PLSR) was used for the quantification of lead. For calibration purposes, different amounts of lead were added to Turmeric samples encompassing a concentration range between 4 and 25 μg g^{-1}. Since lead does not show any Raman band, for the purposes of this study, a complex was formed, its solvent was evaporated and the complex solid samples were registered with a Raman instrument. Raman measurements were performed in two different modes, -diffuse reflectance and transmission-. The PLSR models developed from Raman spectra of two data acquisition modes were evaluated in order to determine the suitability of both acquisition modes for quantifying lead content. The results indicated that diffuse reflectance showed better performance in terms of accuracy and robustness with a bias of 0.55 μg g^{-1}, a relative standard error of prediction (RSEP) of 8.5% and a correlation between the predicted and reference values (R^2) of 0.967. Despite the low lead concentration in the samples, the proposed model allows the quantification of the lead content in a fast and simple way.

1. Introduction

In this article, special emphasis was placed on lead, which is one of the most common heavy metals produced from human activities. Health problems caused by exposure to heavy metals are a worldwide concern. In developing countries, industrial growth and increases in community population result in high volumes of wastewater and environmental pollutants [1]. The different sources of this environmental pollutant include mining, smelting, manufacturing and recycling activities. Lead is also used in many other products such as pigments, paints, solder, stained glass, lead crystal glassware, ammunition, ceramic glazes, jewelry, toys and some cosmetics [1,2]. Heavy metals that contaminate the environment can enter the human food chain through plants, especially plants with underground stems that are consumed [1,3]. Heavy metals can stimulate the production of reactive oxygen species (ROS) and reactive nitrogen species (RNS) through Fenton's reaction. ROS and RNS will be eliminated by the antioxidant defense system. However, the overproduction of ROS and RNS will be beyond antioxidant balancing and lead to oxidative stress conditions, eventually causing damage to tissues and organs [4,5].

Human beings and particularly young children are vulnerable to the toxic effects of lead and can suffer serious and permanent adverse health effects. Some of these effects can include the impaired development of the brain and nervous system. Lead can also cause long-term harm in adults, including increased risk of high blood pressure and kidney damage. The exposure of pregnant women to high levels of lead can cause miscarriages, stillbirth, premature birth and low birth weight [6].

For these reasons, all kinds of products must be assessed in order to protect human beings from dangerous lead quantities. In Thailand, the quality of herbal medicine was set for the limit of products containing heavy metals. Allowed limits of heavy metals in herbal medicinal products are no more than 0.3 μg g^{-1}, 4.0 μg g^{-1} and 10.0 μg g^{-1} for cadmium, arsenic, and lead, respectively [7]. Standard methods used for lead quantification are based on atomic absorption spectrometry (AAS) and inductive coupled plasma (ICP) instruments [8,9]. Although these instruments can provide accurate and precise results, the cost of analysis per sample is quite high, and the sample must be submitted for examination to a laboratory.

* Corresponding author.
E-mail address: jcruz@euss.es (J. Cruz).

https://doi.org/10.1016/j.chemolab.2020.103994
Received 4 October 2019; Received in revised form 4 March 2020; Accepted 5 March 2020
Available online 6 March 2020

The modern Raman spectrometer is interesting since it allows non-destructive analysis [10] and high sample throughput. In addition, portable Raman instruments can be used on-site in agricultural areas. Raman spectral data combined with multivariate regression methods have been reported for the determination of heavy metals in different kinds of samples [10–12]. Normally, surface-enhanced Raman scattering (SERS) is often used to enhance the Raman signal of heavy metals [13–19]. However, commercial SERS materials have been not widely available. In this study, a Raman spectrometry combined with the partial least squares regression (PLSR) [20–23] approach was developed for the determination of lead contents in Turmeric (*Curcuma longa* Linn.) samples. Turmeric was selected to study because several countries including Thailand use it as a medicinal herb and food additive. It is also an important ingredient in several Asian countries. Moreover, the adulteration of lead chromate to Turmeric is a worldwide food safety concern. The lead contents in these samples were prepared into simple complex forms [12] before Raman measurements. The PLSR models developed using two data acquisition techniques, diffuse reflectance, and transmission, were compared.

2. Materials and methods

2.1. Chemical reagents

Lead standard solution, potassium thiocyanate (analytical grade) and nitric acid (analytical grade) were purchased from Merck (Germany). Manganese (II) chloride tetrahydrate was obtained from Sigma-Aldrich (USA) and made into a 1 g L^{-1} solution. Potassium thiocyanate was prepared in deionized water to make a 10 g L^{-1} solution. 1,10-Phenanthroline monohydrate was from Loba Chemie (India) and prepared into 3 g L^{-1} solution with methanol. Sodium hydroxide was purchased from Carlo Erba reagents (Italy). Whatman filter paper No.1 was used to filter the complex precipitate.

2.2. Samples preparation

Turmeric powder was used for sample preparation and it was obtained from an organic garden in Srakauw province of Thailand. This powder was checked for heavy metal contents (Pb, As, Cd) by ICP-OES before using. The results showed that the contents of heavy metal were not found in the detection limit of ICP-OES. After checking, this powder was enrolled and used throughout the study. Lead was added to the samples in a complex form in order to boost the Raman signal.

Forty-two samples were prepared by adding specific amounts of turmeric and lead in order to span the concentration between 4 and 25 μg g^{-1}.

The 42 different concentration samples were prepared by accurately weighing 1 g of turmeric powder. Then 10 mL of 10% HNO_3 was used to extract the sample. The filtrate was filtered and a certain volume of the standard solution of lead (10 μg mL^{-1}) was added to 5 mL of the filtrate. Then, the carrier precipitate reagents were added in the following order, 9 mL of manganese chloride (1g·L^{-1}), 14 mL of 1,10-Phenanthroline monohydrate in methanol (3g·L^{-1}) and 6 mL of potassium thiocyanate (10 g L^{-1}). The reaction mixture was mixed and kept for 30 min at room temperature in order to obtain the precipitated lead complex.

The precipitate was filtered and dried at room temperature for 6 h. Further compositions information of the 42 samples can be found in Supplementary data.

2.3. Hardware and software

A Raman spectrometer (Horiba Scientific, Japan) was used throughout the study. A visible laser of 785 nm was used as the excitation source. The optical microscope was used with a 60 times power objective. The resolution of the grating was set at 0.5 μm. The Raman instrument was controlled by LabSpec version 6.4.4.16 software. Multivariate calibration models were constructed using The Unscrambler ® 10.3 from CAMO Analytics (Trondheim, Norway).

Table 1
Measurement parameters for Transmission and Diffuse reflectance Raman spectroscopy modes.

Parameter	Diffuse reflectance mode	Transmission mode
Acquisition time	10 s	30 s
Accumulations	3	3
Objective lens	50x	–
Neutral density filters	5%	100%
Confocal hole	1000.03	1000.03
Collection	microscope	transmission
Range	50-4000 cm^{-1}	50-4000 cm^{-1}

2.4. Reference method

Heavy metal concentrations of each sample used as reference were measured by inductively coupled plasma-optical emission spectrometer (ICP-OES) based on AOAC (2016) method 999.10 [8]. Five milliliters of the filtrate extracted fraction from the sample preparation above was added to the standard solution to obtain 4–25 μg g^{-1} of turmeric powder. The solution was digested with concentrated nitric acid at a temperature of 150 °C over 2 h. The resulting solution was diluted and mixed with water to reach a volume of 10 mL. The solutions were analyzed with an ICP-OES.

2.5. Recording of spectra

The spectra recorded with the Raman spectrometer of Horiba Scientific instrument (Horiba Scientific, Japan) were obtained by two different acquisition modes, diffuse reflectance, and transmission. The acquisition parameters for each mode are shown in Table 1.

The lead-complexes were crushed and compressed using a hydraulic press device with a force of 10,000 pounds for 30 s in order to form a circular disc.

The samples were then transferred to a Raman instrument for diffuse reflectance and transmission measurements. The Raman spectra are generated by a 785 nm (red) wavelength laser with DV (Deviation Angle) with a diffraction grating of 500 nm. The typical Raman spectrum obtained from diffuse reflectance and transmission modes were illustrated in Fig. 1.

In addition, the measurement reproducibility of a sample sheet was approved by 10-times repeat measurements of a sample disc f 10 μg g^{-1} of lead co-precipitate complex, and acceptable standard deviation values of these measurements were obtained. It was seen that the good reproducibility was observed for 10 repeat measurements (this can be observed in a figure added into the supplementary material).

2.6. Construction of models

Several spectral pretreatments were tested for calibration models calculations. These spectral pretreatments include Savitzky-Golay Derivatives (second-order polynomial fitting) with 11 to 21-point window [24] and the Standard Normal Variate (SNV) [25].

After the spectral pretreatments were applied to the raw data the samples were evaluated using principal component analysis (PCA). The samples were divided into calibration and validation set by using the algorithm of Kennard and Stone [26].

Calibration models were constructed by using the PLSR algorithm and internally validated by cross-validation (the leave-one-out method). The optimum number of factors to be included were determined from a plot of the explained variance against the number of factors. The initial model thus obtained was refined by selecting different spectral ranges that give as a result the lowest relative standard error for prediction (RSEP) for the validation set.

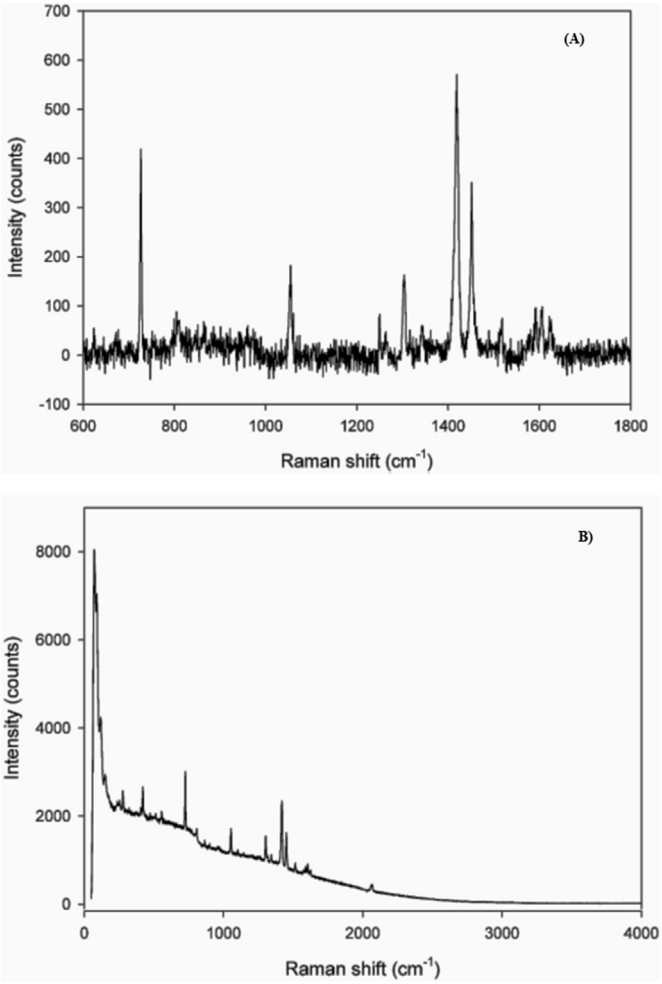

Fig. 1. The typical Raman spectrum obtained from (A) transmission mode and (B) diffuse reflectance mode.

The quality of calibration models and its predictive ability is usually evaluated with the following figures of merit: relative standard error (RSE) and root mean square error (RMSE), which are designated RSEC and RMSEC for calibration and RSEP and RMSEP for prediction, respectively:

$$RSE(\%) = 100\sqrt{\frac{\Sigma_{i=1}^{m}\left(y_{pred} - y_{ref}\right)^2}{\Sigma_{i=1}^{m}\left(y_{ref}\right)^2}} \quad (1)$$

$$RMSE = \sqrt{\frac{\Sigma_{i=1}^{m}\left(y_{pred} - y_{ref}\right)^2}{n}} \quad (2)$$

where **n** is the number of samples used, y_{ref} is the parameter value provided by the reference method and y_{pred} is provided by the Raman spectroscopic method.

3. Results and discussion

In this work, Raman spectroscopy was used for quantifying the lead in turmeric powder.

The concentrations of lead in turmeric powder samples from different sources can vary from zero to very high concentrations. This variation can be caused by several factors. If the turmeric was grown in a lead-contaminated area, the rhizome of turmeric could be exposed and absorb the contaminated lead from soil and water. In these situations, high lead concentrations might be found in the turmeric plant.

On the other hand, lead content may be found in very little or zero amounts in the samples from the non-contaminated area. There was also another concern. Adulteration of lead chromate into turmeric was an important problem in several countries, especially USA and Bangladesh. Lead contents in turmeric samples from Bangladesh were in a range from several hundred up to 1152 μg g^{-1} [27–29]. By looking for the normal lead concentration range in turmeric plants in these articles [27–29], the concentration range 4–25 μg g^{-1} of lead was set in our study. This would be reasonable range and allowed trace analysis of lead content.

3.1. Raman spectra of co-precipitation complex

As it was mentioned in the abstract, since lead does not show any Raman band for overcoming this problem in this study, a trace amount of lead was evaluated as a co-precipitated with the carrier precipitate (manganese-phenanthroline-thiocyanate). In fact, co-precipitation is a widely used process for separation of trace elements from various types of samples [30,31]. Co-precipitation requires a carrier precipitate for collection of trace elements. There are at least four mechanisms involved in the co-precipitation process, i.e., surface adsorption, occlusion and inclusion, mixed crystal formation and post precipitation. Among these, surface adsorption is the major process when co-precipitation occurs [31]. So, this perhaps is the co-precipitation mechanism of lead with the carrier manganese-phenanthroline-thiocyanate. This assumption was supported by the mole ratio of carrier precipitate reagents used in the experiment condition. Potassium thiocyanate was used much more than phenanthroline and manganese chloride. When the precipitate was formed, the excess thiocyanate anions would be adsorbed as the primary layer on the surface of precipitate. Thus, the ions with opposite charge including lead could be adsorbed on the surface as the second counter ions layer to complete charge neutralization. Actually, Raman peaks of the co-precipitate were contributed from the functional groups of phenanthroline and thiocyanate. Raman spectrum of the carrier manganese-phenanthroline-thiocyanate complex was changed from the spectrum of phenanthroline ligand since the new peaks presented a shift to a few wavenumbers (Fig. 2) [12]. In the presence of lead ions, the adsorbed ions on the surface of co-precipitate could enhance the polarization of Raman signal [12]. The intensities of Raman peaks at 726 cm^{-1} and 1452 cm^{-1} were significantly increased, and this increased in peak intensity was concentration dependent (see Fig. 3).

The interferences from the matrix of the turmeric sample were also studied by comparing Raman spectra of the turmeric sample with the co-precipitate complex of lead standard only and co-precipitate complex of lead standard spiked turmeric sample. As shown in Fig. 4, the matrix in the turmeric sample has not interfered with the co-precipitation of lead and Raman spectrum of co-precipitate of lead spiked turmeric was similar to Raman spectrum of co-precipitate of lead at 10 μg g^{-1}.

3.2. Modelling strategy

The original data from the diffuse reflectance and transmission modes were pre-treated by means of SNV for reducing the noise and baseline drift of the spectra.

After pretreatment of the spectra, different PCA analysis of the SNV data were performed, and the samples were evaluated for reasonable sample grouping according to their concentrations. The score plots from the PCA in Fig. 5 were observed in three groups, however, they did not show direct grouping relations with the lead concentration from each one of the samples.

To ensure accurate predictions, a calibration model should encompass all possible variability sources for the body of samples to be determined. To identify the samples meeting these criteria, we applied the Kennard-Stone algorithm to the sample sets available. By this methodology, 31 of the 42 samples were selected by means of Kennard and Stone sample selection [26] and used as calibration set samples. The remaining

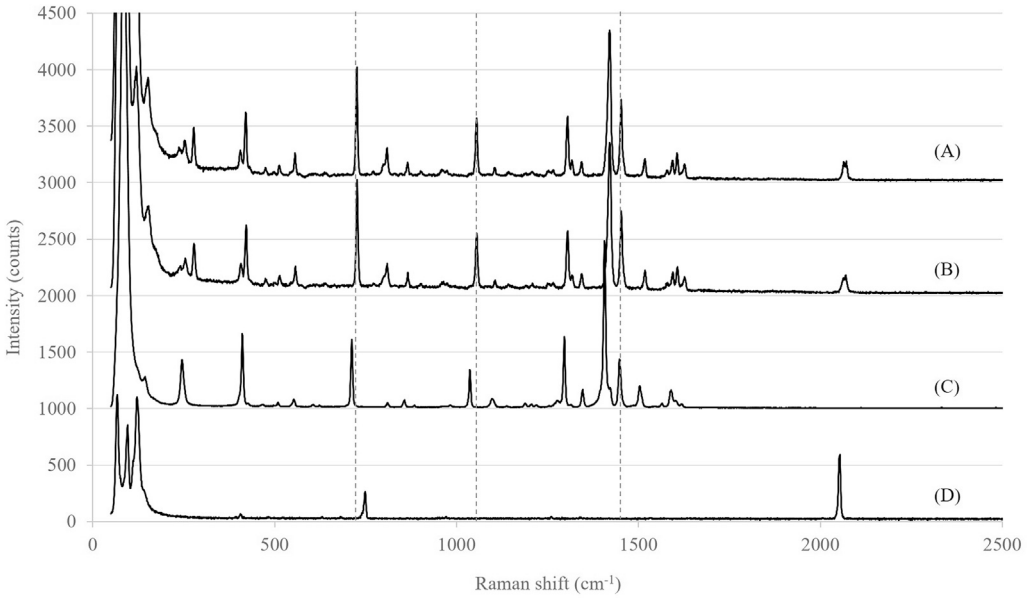

Fig. 2. (A) Raman spectrum of lead co-precipitation complex, (B) Raman spectrum of co-precipitate complex without lead, (C) Raman spectrum of 1,10-phenanthroline and (D) Raman spectrum of KSCN.

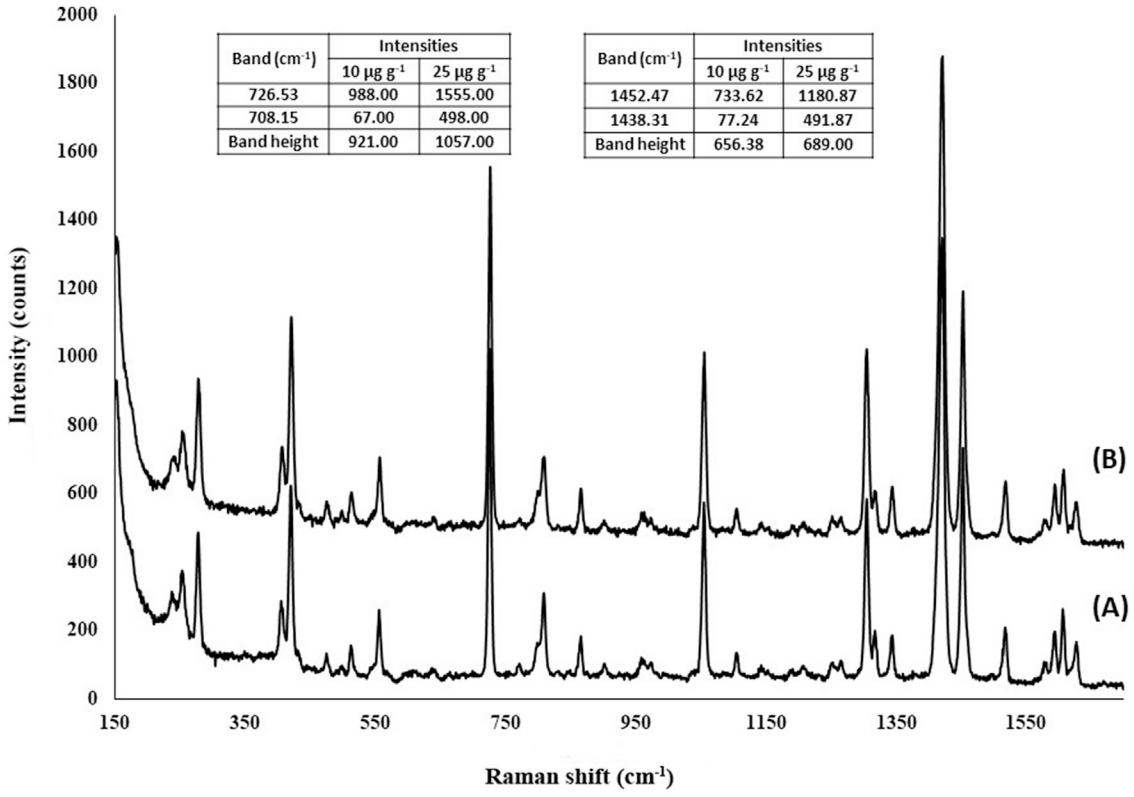

Fig. 3. Raman spectra lead co-precipitate complex concentrations (A) 10 µg g^{-1} and (B) 25 µg g^{-1}.

11 samples were used as the validation set and used to test the prediction efficiency of the model.

From the scores of the scatter plot (PC1 vs PC2) obtained from a PCA of samples for transmission and diffuse reflectance spectra as shown in Fig. 5, it can be seen that the 11 selected as validation samples encompassed the whole spectral variability of those used for calibration. These selected samples were evaluated to span the whole concentration range for a homogeneous distribution of concentrations. This process occurred so that the addition of more samples to our calibration sample set for validation was not necessary.

Then, PLS models were constructed by using the whole spectral range (50-4000 cm^{-1}). Various treatments (SNV, first and second derivative) were performed and compared the results. As showed in Table 2 and Table 3, the optimum model for diffuse reflectance mode was obtained using SNV pre-treated data, while SNV plus 1st Savitzky-Golay derivative with 11 points window was the best data treatment method for

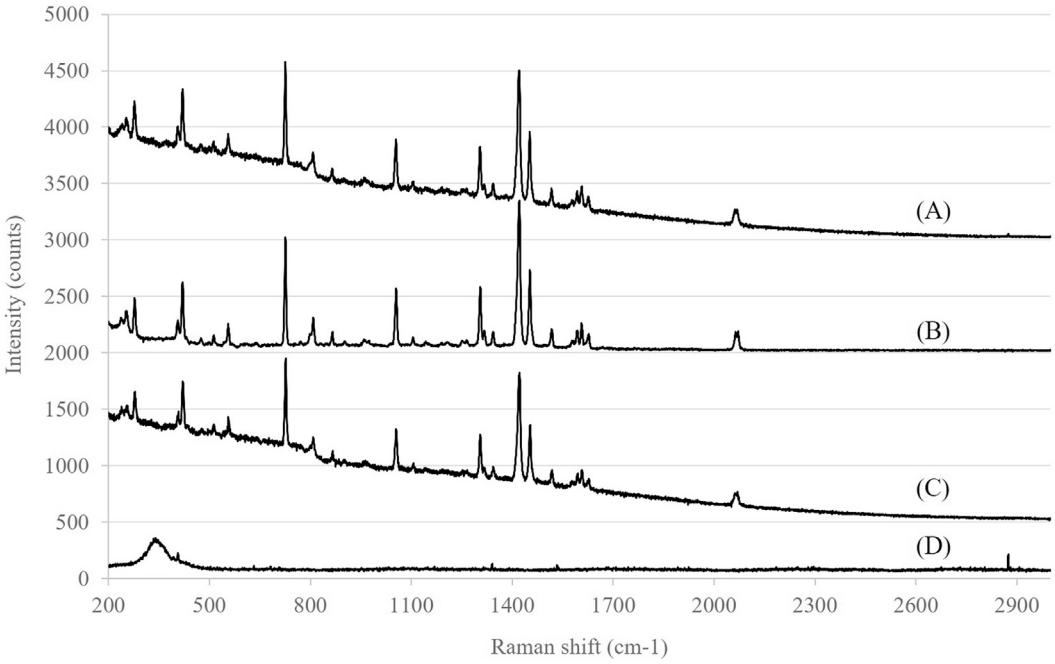

Fig. 4. Raman spectra of: (A) co-precipitate complex of lead standard (10 μg·g-1), (B) co-precipitate complex of lead standard (10 μg·g-1) spiked turmeric sample, (C) co-precipitate complex without lead spiked turmeric sample and (D) turmeric sample.

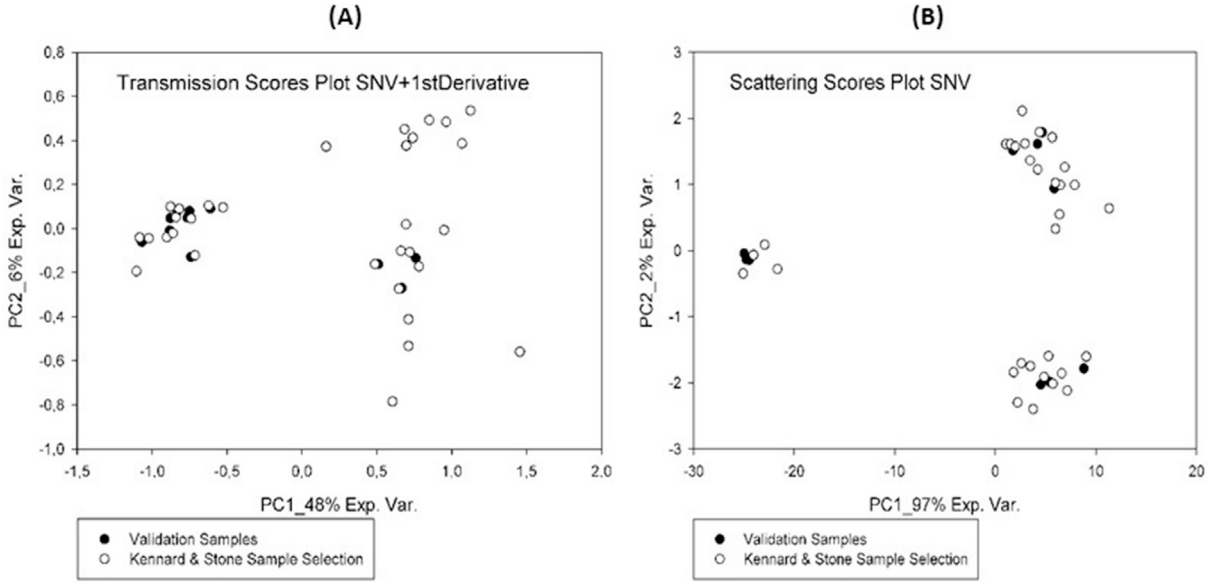

Fig. 5. The scores of the scatter plot (PC1 vs PC2) from a PCA of samples for (A) transmission spectra with SNV plus 1st Derivative pretreatment and (B) diffuse reflectance spectra with SNV pretreatment. The symbol (•) stands for a validation sample and (°) stands for a calibration sample selected by Kennard & Stone algorithm.

transmission mode. The intensities of Raman peaks at 726 cm^{-1} and 1452 cm^{-1} were other items for selecting the best spectral range but, the optimum spectral range was identified by using the jack-knifing criterion [32], which shows the variables that most strongly influence the performance of a model.

Fig. 6 shows that Jack-Knifing criterion is marking for the diffuse reflectance PLS model, the range between 50 and 824 cm^{-1} as the variable range with the most influence to the lead complex quantitation, and the range that performs better predictive models. Despite there being a few more marked variables up to 824 cm^{-1}, the models containing this range do not provide better results.

Application of these criteria provided the ranges listed in Table 4 and Table 5, which coincided with those containing the major bands of the spectra for the lead complex. The optimum models were employed for spectral ranges between 50 and 824 cm^{-1} and 800–1150 plus 1250–1650 cm^{-1} for the diffuse reflectance mode and the transmission mode, respectively. Samples that showed a high value of sample leverage, X or Y variance residuals were considered outliers if the residual values do not decrease after adding one PLS factor to the plot variance residuals vs. sample leverage and were excluded from the calibration models.

The optimum PLSR models will have the lowest number of PLS factors and appropriate model parameters, i.e., bias value, RMSE, and RSE. In addition, the correlation between the reference values and predicted

Table 2
The merit for calibration and validation sets of Pb-complex by PLS model made with transmission Raman spectra from the full ranges (50-4000 cm^{-1}).

Pretreatments	–	SNV	1st Derivative	2nd Derivative	SNV+1st Derivative	SNV + 2nd Derivative	1st Derivative + SNV	2^{nd}Derivative + SNV
Spectral range (cm^{-1} (	50–4000							
Calibration Samples	31	31	31	31	31	31	31	31
Number of latent factors	2	5	5	2	4	6	4	5
Explained Y variance (%)	78.31	99.55	96.90	78.74	99.14	99.87	98.36	99.70
RMSEC ($\mu g \cdot g^{-1}$ (	3.06	0.44	1.16	3.03	0.61	0.23	0.84	0.36
RSEC (%)	20.37	2.93	7.70	20.17	4.05	1.57	5.60	2.40
Validation Samples	11	11	11	11	11	11	11	11
BIAS ($\mu g \cdot g^{-1}$ (	−2.14	−1.68	−1.75	−1.51	−1.99	−2.28	−2.30	−2.18
RMSEP ($\mu g \cdot g^{-1}$ (	4.68	3.17	3.86	3.66	3.16	3.43	3.53	3.45
RSEP %	29.61	20.04	24.43	23.13	20.01	21.71	22.31	21.83
R^2	0.630	0.861	0.761	0.761	0.881	0.866	0.861	0.849

Table 3
The merit for calibration and validation sets of Pb-complex by PLS model made with diffuse reflectance Raman spectra from the full ranges (50-4000 cm^{-1}).

Pretreatments	–	SNV	1st Derivative	2nd Derivative	SNV+1st Derivative	SNV+2nd Derivative	1st Derivative + SNV	2nd Derivative + SNV
Spectral range ($\mu g \cdot g^{-1}$ (	50–4000							
Calibration Samples	31	31	31	31	31	31	31	31
Number of latent factors	4	4	6	5	4	4	4	4
Explained Y variance (%)	94.51	96.34	99.09	99.09	97.48	99.72	97.83	99.73
RMSEC ($\mu g \cdot g^{-1}$ (	1.54	1.25	0.63	0.63	1.04	0.34	0.97	0.34
RSEC (%)	10.24	8.37	4.17	4.17	6.94	2.28	6.44	2.29
Validation Samples	11	11	11	11	11	11	11	11
BIAS ($\mu g \cdot g^{-1}$ (	−0.11	−0.54	−1.53	−0.05	−0.62	−0.64	−0.64	−0.57
RMSEP ($\mu g \cdot g^{-1}$ (	1.39	1.34	1.76	2.47	1.61	2.23	1.51	2.31
RSEP %	8.78	8.50	11.11	15.65	10.18	14.08	9.53	14.62
R^2	0.959	0.967	0.934	0.880	0.952	0.917	0.960	0.907

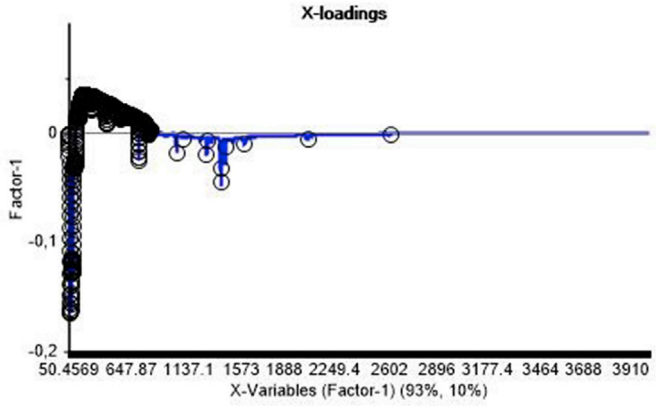

Fig. 6. 1st PLS factor loading plot for diffuse reflectance model (range of 50–4000 cm^{-1}), where the application of the Jack-Knifing criterion which shows the variables that most strongly influence the performance of the model.

values (R^2) is also an important criterion for consideration.

3.3. Transmission mode model

For the transmission mode, the best model for lead is the one shown in Fig. 7(A), which shows the plot predicted calibration value vs. the reference value. As can be observed in this plot, the model has a slope close to 1 (0.979), an offset close to 0 (0.116), and an R^2 of 0.991, which are good calibration parameters.

Table 4 shows the most salient calibration parameters for the model, as well as the calibration and prediction errors obtained. The pretreatment used for this model is SNV and the 1st Savitzky-Golay Derivative with an 11 points window, and the spectral range is 800–1150, 1250-1650 cm^{-1}.

Table 4
The merit for calibration and validation sets of Pb-complex by PLS model made with transmission Raman spectra from various ranges.

Pretreatments	SNV+1st Savitzky-Golay Derivative 11 with points window			
Spectral range ($\mu g \cdot g^{-1}$ (	800-1150, 1250-1650	700–1650	800–1150	1250–1650
Calibration Samples	31	31	31	31
Number of latent factors	4	4	5	4
Explained Y variance (%)	97.98	99.01	97.20	99.08
RMSEC ($\mu g \cdot g^{-1}$ (	0.93	0.65	1.09	0.63
RSEC (%)	6.21	4.34	7.32	4.19
Validation Samples	11	11	11	11
BIAS ($\mu g \cdot g^{-1}$ (	−1.48	−1.82	−2.71	−1.92
RMSEP ($\mu g \cdot g^{-1}$ (	2.82	3.00	4.42	3.11
RSEP %	17.83	19.00	27.97	19.69
R^2	0.875	0.879	0.745	0.875

Table 5
The merit for calibration and validation sets of Pb-complex by PLS model made with diffuse reflectance Raman spectra from various ranges.

Pretreatments	SNV			
Spectral range ($\mu g \cdot g^{-1}$ (	50–824	825–2500	2500–4000	50–4000
Calibration Samples	31	31	31	31
Number of latent factors	4	4	4	4
Explained Y variance (%)	96.81	98.97	99.38	96.34
RMSEC ($\mu g \cdot g^{-1}$ (	1.17	0.67	0.51	1.25
RSEC (%)	7.81	4.44	3.44	8.36
Validation Samples	11	11	11	11
BIAS ($\mu g \cdot g^{-1}$ (	−0.55	−0.42	−0.31	−0.54
RMSEP ($\mu g \cdot g^{-1}$ (	1.31	2.07	4.86	1.34
RSEP %	8.28	13.11	30.74	8.50
R^2	0.971	0.914	0.491	0.967

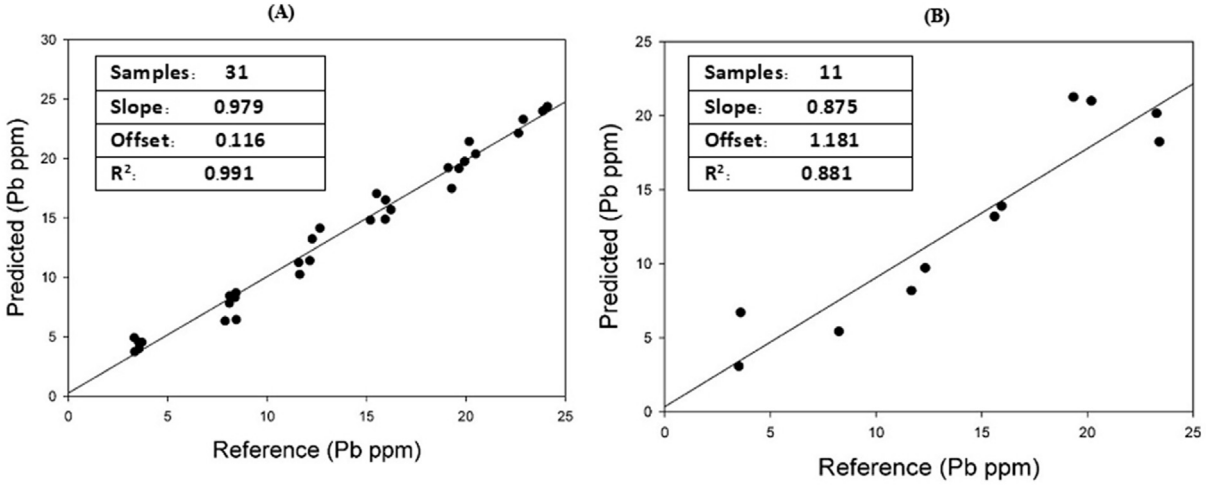

Fig. 7. Calibration curve (A) and validation curve (B) of predicted Pb values vs. reference by PLS model made with transmission Raman spectra.

As seen from Table 4, using 4 PLS factors was enough to obtain a model with the adequate predictive ability for lead; in fact, the resulting RSEP value was less than 17.83%. Despite the good calibration model, the prediction error is larger than 10%, which is not good enough for the medicinal plant industry. The model also has an important bias of −1.48 μg g^{-1} of lead, and a low value of the correlation coefficient in the predicted vs. reference plot of 0.881 as is shown in Fig. 7(B), this result makes it a bad model for lead prediction due to its high prediction errors.

3.4. Diffuse reflectance mode model

For the diffuse reflectance mode, the best model for lead is the model shown in Fig. 8(A). As seen in this plot, the model has a slope close to 1 (0.968), a low offset (0.430), and an R^2 of 0.968, which are good calibration parameters.

Table 5 shows the important calibration parameters for the model, as well as the calibration and prediction errors obtained. The pretreatment used for this model is SNV, and the spectral range is 50–824 cm^{-1}. As seen from Table 5, using 4 PLS factors was enough to obtain a model with the adequate predictive ability for lead, in fact, the resulting RSEP value was less than 10% (8.28%).

The prediction error is less than 10%, and together with a small bias of −0.55 μg g^{-1} of lead and a high value of correlation coefficient in the predicted vs. reference plot of 0.971 as is shown in Fig. 8(B), makes this model suitable for the assessment of the quality of turmeric in the medicinal plant industry.

3.5. Models summary

As seen in Figs. 7–8 and Tables 4 and 5, the PLSR model obtained from the diffuse reflectance and transmission modes expressed a good correlation coefficient (R^2) between the predicted values (Y-axis) and the actual values (X-axis), with R^2 values higher than 0.9. These results indicated that the predicted lead concentrations in the validation set strongly agreed with the actual values from the ICP-OES method. However, the model obtained from the diffuse reflectance mode appears to be better than that obtained from the transmission mode. This finding was the result of the lower bias, RMSE and RSE values of the diffuse reflectance model, compared with those of the transmission model.

In this study, the transmission mode was used for discovering local heterogeneities of the measured samples. Unfortunately, our results showed that the transmission mode was not appropriate for heavy metal complexes since it provided very weak Raman spectral signal as is shown in Fig. 1 (A). For the diffuse reflectance mode, the measurement signal was obtained from the accumulation of multiple scattered radiations from the sample surface. The acquired spectral signal appears clearer and stronger than the signal from the transmission mode, as can be observed in Fig. 1 (B). Therefore, the PLSR model of the diffuse reflectance spectra

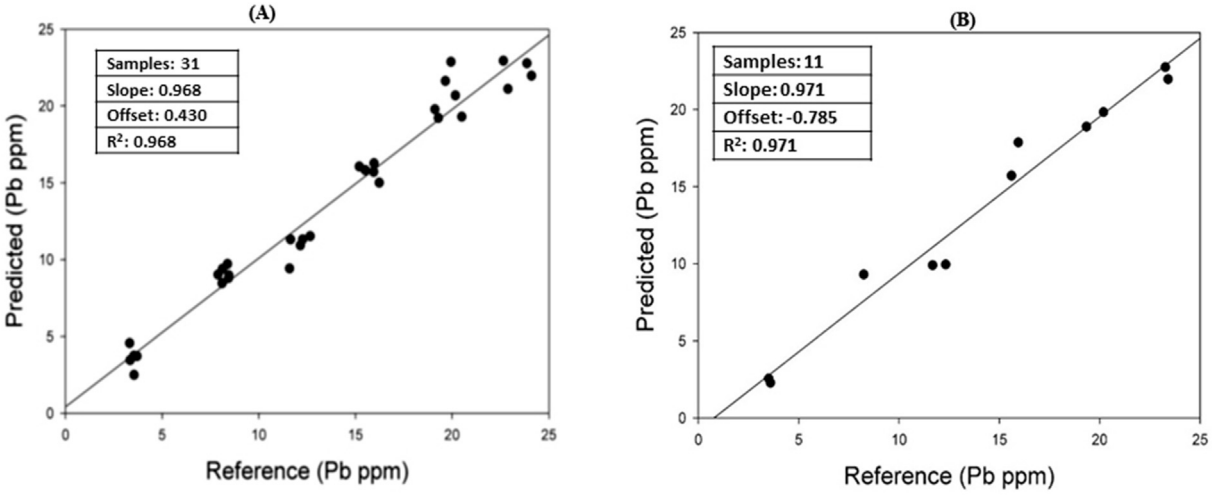

Fig. 8. Calibration curve (A) and validation curve (B) of predicted Pb values vs reference by PLS model made with diffuse reflectance Raman spectra.

was much better than the PLSR obtained for the transmission mode for the quantitative determination of lead content in turmeric powder.

4. Conclusion

The controlled determination of the content of lead ions in turmeric powder by using PLSR models of Raman spectral data was demonstrated. In addition, different data acquisition modes, i.e., diffuse reflectance and transmission, were tested, and the prediction results were compared. High correlation coefficients between the predicted and reference values were obtained for both models. Moreover, the best results of our study showed the diffuse reflectance mode to be the most robust acquisition mode that provided the best prediction results. Despite the low concentration of Pb (4–25 μg g^{-1}), good results have been obtained, with low residual values and a low RSEP of 8.28% for the dataset acquired using the diffuse reflectance mode. A method for quantifying lead content in a fast and simple way was demonstrated with the obtained results.

Declaration of competing interest

The authors declare that they have no known competing financial interests or personal relationships that could have appeared to influence the work reported in this paper.

CRediT authorship contribution statement

Putthiporn Khongkaew: Investigation, Methodology, Validation, Writing - original draft, Formal analysis, Visualization, Writing - review & editing. **Chutima Phechkrajang:** Conceptualization, Funding acquisition, Project administration, Methodology, Writing - original draft, Writing - review & editing, Resources, Validation. **Jordi Cruz:** Conceptualization, Methodology, Supervision, Investigation, Validation, Visualization, Writing - review & editing, Software. **Vanessa Cárdenas:** Formal analysis, Writing - review & editing, Visualization. **Piyanuch Rojsanga:** Data curation, Investigation, Validation.

Acknowledgments

This research was funded by the Ministerio de Economía y Competitividad through the project CTQ 2016-79696-P (AEI/FEDER, EU) and by the Coordinating Centre for Research and Development to Increase Value of the Plants Indigenous to Thailand, Mahidol University, Thailand Research Fund (RDG6020026).

Appendix A. Supplementary data

Supplementary data to this article can be found online at https://doi.org/10.1016/j.chemolab.2020.103994.

References

[1] A.K. Krishna, P.K. Govil, Soil contamination due to heavy metals from an industrial area of Surat, Gujarat, Western India, Environ. Monit. Assess. 124 (2007) 263–275.
[2] P. Miskowiec, et al., Soil pollution with heavy metals in industrial and agricultural areas: a case study of Olkusz District, J. Elem. 20 (2) (2015) 353–362.
[3] I. Kosalec, et al., Contaminants of medicinal herbs and herbal products, Arh. Hig. Rada. Toksikol. 60 (2009) 485–501.
[4] M. Jaishankar, et al., Toxicity, mechanism and health effects of some heavy metals, Interdiscipl. Toxicol. 7 (2) (2014) 60–72.
[5] M. Valko, et al., Redox- and non-redox-metal-induced formation of free radicals and their role in human disease, Arch. Toxicol. 90 (2016) 1–37.
[6] W. Ab Latif, et al., Lead toxicity: a review, Interdiscipl. Toxicol. 8 (2) (2015) 55–64.
[7] Department of Medical Sciences, Thai Herbal Pharmacopeia, vol. III, Nonthaburi: Department of Medical Sciences, Ministry of Public Health, 2009.
[8] Aoac Authors, Official Methods of Analysis Minerals Analysis *Lead, Cadmium, Zinc, Copper, and Iron in Foods*, twentieth ed., Association of Analytical Communities, Gaithersburg, MD, 2016. Reference data: Method 999.10 (9.1.08).
[9] B. Mikula, et al., Application of 1,10-phenanthroline for preconcentration of selected heavy metals on silica gel, Microchim. Acta. 166 (2009) 337–341.
[10] A. Gredilla, et al., Non-destructive Spectroscopy combined with chemometrics as a tool for Green Chemical Analysis of environmental samples: a review, TrAC Trends Anal. Chem. (Reference Ed.) 76 (2016) 30–39.
[11] E. Gerbino, et al., Use of Raman spectroscopy and chemometrics for the quantification of metal ions attached to *Lactobacillus kefir*, J. Appl. Microbiol. 112 (2) (2012) 363–371.
[12] Y. Liu Y, et al., Determination of copper, zinc, cadmium, and lead in water using co-precipitation method and Raman spectroscopy, 06(03), J. Innov. Opt. Health. Sci. (2013) 1350021, 8 pages.
[13] A. Eshkeiti, et al., Detection of heavy metal compounds using a novel inkjet printed surface-enhanced Raman spectroscopy (SERS) substrateЭ, Sensor. Actuator. B Chem. 171 (2012) 705–711.
[14] A.Y. Panarin, et al., Determination of antimony by surface-enhanced Raman spectroscopy, Appl. Spectrosc. 68 (3) (2014) 297–306.
[15] B. Gu, C. Ruan, Determination of technetium and its speciation by surface-enhanced Raman spectroscopy, Anal. Chem. 79 (6) (2007) 2341–2345.
[16] H. De, et al., Theoretical study of Au4 thymine, Au20 and Ag20 uracil and thymine complexes for surface enhanced Raman scattering, Comput. Theor. Chem. 1111 (2017) 1–13.
[17] E. Tan, et al., A novel surface-enhanced Raman scattering nanosensor for detecting multiple heavy metal ions based on 2-mercapto isonicotinic acid functionalized gold nanoparticles, Spectrochim. Acta. A Mol. Biomol. Spectrosc. 97 (2012) 1007–1012.
[18] M. Ricci, et al., The Raman and SERS spectra of indigo and indigo-Ag2 complex: DFT calculation and comparison with experiment, Spectrochim. Acta. A Mol. Biomol. Spectrosc. 188 (2017) 141–148.
[19] B. Hayati, et al., Super high removal capacities of heavy metals (Pb^{2+} and Cu^{2+}) using CNT dendrimer, J. Hazard Mater. 336 (2017) 146–157.
[20] H. Martens, T. Naes, Multivariate Calibration, Wiley, London, 1989 (chapters 2 and 7).
[21] D. Kleinbaum, L. Kupper, K. Muller, Applied Regression Analysis and Other Multivariate Methods, second ed., Pws-Kent, Boston, 1988.
[22] D.L. Massart, et al., Handbook of Chemometrics and Qualimetrics: Part B, Elsevier, The Netherlands, 1998, pp. 349–379.
[23] O.E. De Noord, Multivariate calibration standardization, Chemometr. Intell. Lab. Syst. 25 (1994) 85–97.
[24] A. Savitzky, M.J.E. Golay, Smoothing and differentiation of data by simplified least squares procedures, Anal. Chem. 36 (8) (1964) 1627–1639.
[25] R.J. Barnes, et al., Standard normal variate transformation and de-trending of near-infrared diffuse reflectance, spectra, Appl. Spectrosc. 43 (5) (1989) 772–777.
[26] R.W. Kennard, L.A. Stone, Computer-aided design of experiments, Technometrics 11 (1969) 137–148.
[27] J.E. Forsyth, et al., Turmeric means "yellow" in Bengali: lead chromate pigments added to turmeric threaten public health across Bangladesh, Environ. Res. 179 (2019) 108722.
[28] W. Cowell, et al., Ground turmeric as a source of lead exposure in the United State, Publ. Health Rep. 132 (3) (2017) 289–293.
[29] J.E. Forsyth, et al., Sources of blood lead exposure in rural Bangladesh, Environ. Sci. Technol. 53 (2019) 11429–11436.
[30] N. Bader, et al., Co-precipitation as a sample preparation technique for trace element analysis: an overview, Int. J. Chem. Sci. 12 (2) (2014) 519–525.
[31] K. Inagaki, et al., Coprecipitation in trace element analysis, encyclopedia of analytical chemistry, R.A. Meyers (Ed.), Chapter September (2009), John Wiley & Sons Ltd.
[32] H. Martens, M. Martens, Modified Jack-Knife estimation of parameter uncertainty in bilinear modeling by partial least squares regression (PLSR), Food Qual. Prefer. 11 (2000) 5–16.